Machine Vision and Applications (1991) 4:263–270

Machine Vision and Applications

Dedicated Image Analysis Techniques for Three-Dimensional Reconstruction from Serial Sections in Electron Microscopy

Ph. Gremillet, and M. Jourlin
Laboratoire de Traitement du Signal, Université de Saint Etienne and ICPI Lyon, France

Cph. Bron and J. Schüpbach
Swiss National Center for Retroviruses, Institut for Immunology and Virology Gloriastrasse, Zürich, Switzerland

H.P. Gautschi and Th. Bächi
Electron Microscopy Laboratory, University Zürich, Institut for Immunology and Virology Gloriastrasse, Zürich, Switzerland

Abstract. This article describes the digital treatments needed to reconstruct spatial information at a 40-nm depth resolution of entire cells from transmission electron microscopic images of serial sections containing laser-induced topographical references. The use of a scanning transmission electron microscope (STEM) allows the acquisition of images with high contrast and good resolution at medium magnification. The scanning of our specimens at video frequencies is an attractive way to link a STEM with an image processing system. The magnetic hysteresis of the spools responsible for the electron scanning induces image deformations that have to be modelized and rectified before registering the images corrected for cutting-induced deformations.

Key Words: image treatment, serial sections, laser references, three-dimensional reconstruction, scanning transmission electron microscopy

1 Introduction

The volume information of a biological object, prepared and embedded for transmission electron microscope observation, is lost during the thin or ultra thin cutting procedure of the polymer block. The digital processing of electron microscopic images from serial sections makes possible the reconstruction of information set prior to serial cutting (e.g., laser-induced topographical references). The extrapolation of the mathematical calculations for the reconstruction can be applied to the surrounded material containing unknown information (e.g., a serially sectioned cell). This technique allows us to reconstruct the three-dimensional information contained in the microscopical sections and the depth resolution is the section's thickness. We have already demonstrated the feasibility of this technique for transmission electron microscopy (TEM) coupled with a video camera (Bron et al. 1990a,b). In order to get images with higher contrast and better resolution at medium magnification, we decided to use a scanning transmission electron microscope (STEM). The electron probe of this type of transmission electron microscope is not coherent or parallel but focuses on the specimen and enables the generation of electron-induced signals from a very localized area. The dynamically scanned probe produces analog signals displayed at the same scanning rate on a cathode ray tube (CRT). At video frequencies the electronic spools responsible for the microscope scanning are subject to magnetic hysteresis, which induces deformations of the images.

Once the image deformation artifacts caused by the use of STEM are modelized and rectified, the geometrically corrected serial sections can be automatically registered. The normalization of the grey level of each image delivers the necessary homogeneous grey-level distribution throughout the reconstructed block. This is obtained by logarithmic processing (Jourlin and Pinolli 1988) of the original grey-level information.

Address reprint requests to: Cph. Bron, Swiss National Center for Retroviruses, Institut for Immunology and Virology Gloriastrasse, 30 8028 Zürich, Switzerland.

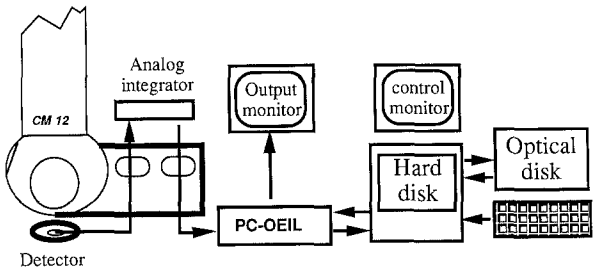

Figure 1. The EM bright field images taken with a Philips CM 12 STEM were directly processed at the TV scan rate. They were analogically integrated, then digitized and memorized on optical disks.

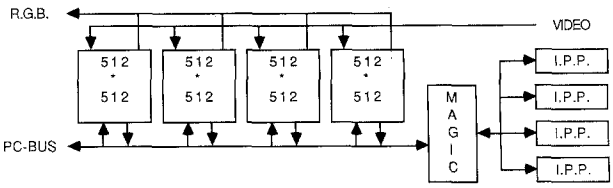

Figure 2. The PC-OEIL™ board is a completely self-sufficient image-processing hardware with four 512*512*8 bits frame buffers and four data flow processors (Image Pipelined Processors μPD7281 from NEC). The board is plugged into any 16 bits slot of an IBM PC AT 03™ or another compatible computer.

The reconstructed spatial information can then be visualized, analyzed, and quantified at EM magnifications. This technique paves the way toward the use of the single cell as the reagent tube.

2 Requirements

2.1 Microscope

The EM bright field images taken with a Philips CM 12 STEM were directly processed at the TV scan rate (see Figure 1). The analog signal was integrated 32 times (Hamamatsu DS 6000) to enhance the signal-to-noise ratio. A test grid with parallel lines at 0.463 μm allowed the determination of the compression of the images. The test grid, once centered, was rotated 90° by means of a rotation holder introduced into the EM column without changing the alignment. The comparison of the images allowed the determination of the real magnification in X and Y.

2.2 Computer

Video images were digitized to a density of 512 × 512 pixels and the following image analysis and treatments shown in Figure 2 were made with a PC-OEIL™ board.* This electronic board is plugged into any 16-bit slot of an IBM PC AT 03™ or another compatible computer. The PC-OEIL™ board is completely self-sufficient, image processing hardware. It contains all the functions required to digitize, process, and visualize images. The board has four 512*512*8-bit frame buffers. The third and the fourth frames can be reorganized to offer 16 binary frames to the user. It has four data flow processors (Image Pipelined Processors μPD7281 from NEC). All the treatments on the images are assumed at high speed by the IPPs. The board uses the IBM-PC bus architecture to communicate with other processors. The PC drives the board and stores the digitized data on optical disks (IBM™ 3363), each of 200-Mbyte memory capacity.

3 Implementation

3.1 Image Restoration

3.1.1 Electronic image compression. The electronic image compression effects are linked to the angular acceleration of the scanning speed of the electron beam. The scanning of the electron beam is induced by the magnetic fields of two concentric pairs of spools perpendicularly oriented to the electron beam axis in the upper part of the electron microscope column. The deformations of the later digitalized image are made visible because the electronic image on the cathode ray tube (CRT) is the result of electrostatic-driven scanning. It is difficult if not impossible to obtain a similar scanning from magnetic scanning of an electron beam with adequate potential for transmission electron microscopy (10 to 120 KeV) and electrostatic scanning of a CRT electron beam (Figure 3). A test grid with parallel grating lines at 0.463 μm was rotated along two or more angles to determine the image deformation parameters. We found no irregularity in the grating when the lines were horizontally oriented, and thus did not apply any vertical correction. There was some distortion in the image when the grid was rotated so that the grating lines were vertically oriented: The distances between any two consecutive lines were not constant; the distortion was a nonlinear compression on the left half of the image, which was consistent with the fact that the compression along the X axis of the image was proportional to the acceleration of the scanning speed of the electron beam. This acceleration caused a magnification

* The PC-OEIL board's software is developed by MISIS-Image. The software and hardware are commercially available upon request to: MISIS-Image, 10 bis, rue de la Productique F-42100, Saint-Etienne, France.

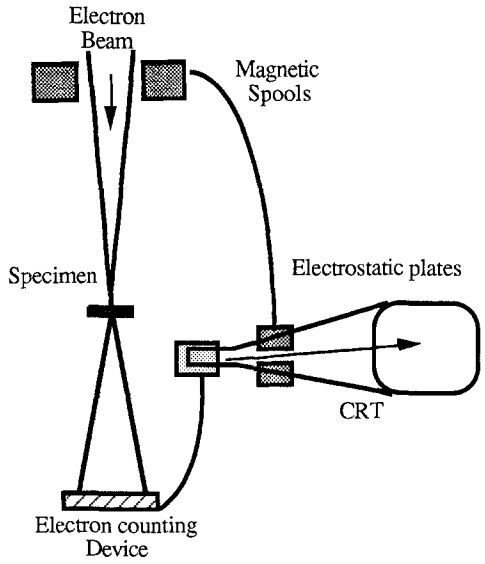

Figure 3. Schemata of the STEM. The scanning of the electron beam is induced by the magnetic spools in the upper part of the electron microscope column. The deformations are made visible because the electronic image on the cathode ray tube (CRT) is the result of an electrostatic-driven scanning. The digitized image at video rate scanning is the same as the CRT image.

difference between two different points of the same line. (Figure 4*A*). The precision obtained was proportional to the mean distance calculated on the right-hand part of the image (see Figure 4B). Although the implemented method is different from the theoretical basis of the deformation, it produces good results because the mean distance first computed is 8 pixels. In terms of software, such a test grid method was easy to write and fast during execution (a few seconds per image). This test controls the electron microscope from the standpoint of the resulting images and is independent of the chosen tension and alignment settings.

3.1.2 Rotational scanning distortion. A more complex deformation occurs with the rotation of the scanning direction. The rotation of scanning is associated with the modulation of the signal producing the magnetic fields responsible for the electron beam deviation. The signal in the spools previously mentioned is modulated by sine and cosine functions in order to direct the electron beam according to a rotated direction. The modulation is well stabilized in a slow scan mode so that no sensible deformation is noticed. However, in the TV rate scanning mode the frequency of the frame is 50/sec and the line scan is 52 μsec so that the demagnetization of the spool obtained at the end of a line by an electronic peak is not completed at the beginning of the next line. This phenomenon is called *hysteresis*. The hysteresis of the spool is directly proportional to the intensity of the signal used to deviate the electron beam, that is, directly proportional to the angle of rotation of the scanning. The intensity of the current needed to induce the magnetic field is proportionally adapted to the tension of the electron beam. The resulting images are then compressed according to both the rotation of the scanning and the tension potential.

3.1.3 Translation between rotation center and image center. The image center is linked to the

A

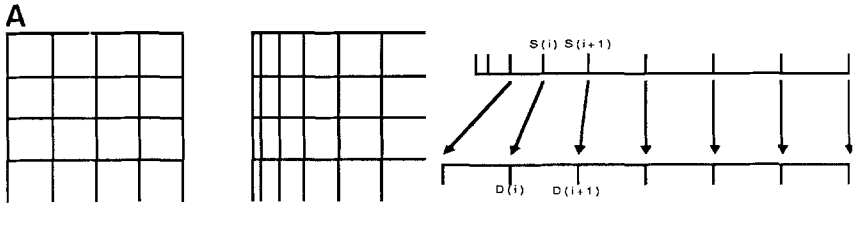

B

1. Extraction of the grey level deflections on an averaged profile issued from a set of consecutive lines.
2. Computation of the mean distance between two deflections on the half-right part of the profile.
3. Determination of a linear transformation to be applied on each couple of deflections of the half-left part.
4. The content of each [S(i),S(i+1)] segment will simply be mapped using a linear interpolation onto the corresponding [D(i),D(i+1)] segment.

Figure 4(A). The angular acceleration difference brings a magnification difference between two different points of the same line. (B) Procedure of electronic deformation calculation with a test grid.

magnetic alignment of the electron lenses in the microscope column. This alignment is different in the TV scan mode and in the slow scan mode. A translation between the two images is the result of the differences between the corresponding alignments. This implies that the center of the STEM image in the TV mode is not the rotation center of the image when a rotation is applied. The translation between the rotation center and the image center has to be known in order to register two similar images taken at different rotation angles. In order to simplify this treatment, whenever possible we avoided rotation of the scanning of our specimen.

3.1.4 Image restoration linked to the physical deformations. Once the electronic deformations were corrected on each image, the physical deformations of adjacent sections had to be corrected in order to make the final registration. The back-calculation to be applied on each cut was performed automatically on the basis of the laser holes or fiducials.

In short, two images corrected for electronic deformations were needed to permit the calculations necessary for image restoration. Image A was the one we wanted to study (at magnification 10,000×). Image B was image A at a lower magnification (3600×), which should contain all three fiducials.

From image B the computer calculated the position of the centers of gravity of the laser holes, and the deformations and orientation deduced from these calculations were then applied to each image A in order to fit it into the reconstructed block.

On the acquired B image, the fiducials could be located at any position on the image, but they formed an orthonormal marker before the cutting procedure, as shown in Figure 5 (top). The model of the geometrical transformation that we used is a first-order affine transform. Such a transform turns a parallelogram into another parallelogram and three laser fiducials are necessary and sufficient. The procedure applied to the images for the computation of the center of gravity and the geometrical correction is described in Figure 5 (bottom).

The physical distortions of the sectioned surface produced by the ultramicrotome are much more complex, but the observed field is about 100 times smaller than the sectioned plane. We decided to limit ourselves to a first-order affine transform using six parameters because, even if reducing the transform to a simple one no longer suits reality, our affine model is still quite a good approximation of the theoretical distortion as demonstrated by the fourth laser fiducial seen in Figure 6A, which is not considered in the registration calculations. In addition, the image analysis system onto which CAVUM (computer-aided volumic ultra-microscopy) is implemented would roughly not be able to perform higher-order transforms in a reasonable amount of time.

3.1.5 Normalization of the images grey-level distributions. Even with perfect cutting techniques, two adjacent sections rarely have the same grey-level distribution. This is due to small variations in the thickness of the cuts that result in different absorption of the electrons. New algorithms based on Jourlin and Pinolli's (1988) model of the logarithmic image processing allowed us to normalize the grey-level distribution through all images and to enhance the contrast of the images in calculating their optimal homothesis. All images have the same grey-level distribution after this automatic mathematical treatment, regardless of the distribution before the treatment. The resulting histograms have the same mean and the same variance. On the images, there is a dark object (the observed cell) and a light background. In the procedure of grey-level normalization (Figure 7), step 3 produced a uniform background while step 4 increased contrast in the interesting part of the scene (the cell itself).

3.2 Image Analysis and Presentation

The EM magnification chosen resulted in picture elements (pixels) of 40-nm length. The cutting procedures allowed a section thickness of 40 nm. The restoration of the third dimension thus yielded cubic volume elements (voxels) of a 40-nm side length. The extraction of a chosen line on every cut reconstructed an image having the same resolution as the original cuts and represented a new cut along another axis, exactly as if the block was cut along this direction (see Figure 8). It was interesting to visualize the scene using the same aspect as that used by electron microscopists. We concentrated our efforts on visualizing strictly orthogonal sections along the block. The presence of four frame buffers on the electronic board to produce images was intentional. The number of the line, the column, and the number of the cut defined the four views so that the system simultaneously built four views of the same block, all stored on the four frame buffers. The user can then switch in real time from one view to another (Figure 6C).

3.3 Performance

3.3.1 Reconstruction time. The calculations leading to the registration of 130 cuts were done in 50 min and performed on site so that the block could

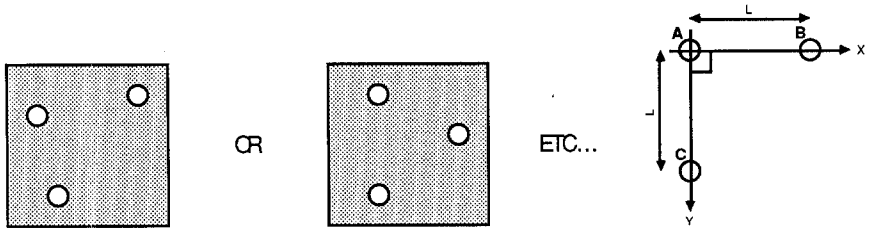

1. Histogram of the grey-level image.
2. Binarization of the image after computation of a grey-level threshold value over which pixels will be turned to white, and under which pixels will be turned to black.
   Computation of the threshold value :
   First: computation of the mean grey-level of the histogram, and then forcing all histogram values lower than the mean value to zero.
   Second: computation of the mean grey-level of the resulting histogram, and then forcing all histogram values lower than the mean value to zero.
   Third: Searching a grey-level value that will maximize the interclass variance between the two obtained classes of the histogram.
   Grey-level values lower than the threshold value are turned to black, the rest been turned to white.
3. The resulting binary image contains all the laser fiducial, and also some noise extracted from the background of the original grey-level image.
4. Noise consists on thin binary objects that are easy to remove, by first creating a marker image by eroding the original binary image with a 7*7 structural element, and then reconstructing the original binary image using this marker.
5. Each present laser fiducial is then extracted by repeatedly searching the first object of the image, computing its center of gravity, subtracting the object from the image, and so on until there is no object left on the image.
6. A center of gravity is a couple of floating-point values (Xg,Yg) where :
   Xg is the sum of all Xi divided by N
   Yg is the sum of all Yi divided by N
   with :
   (Xi,Yi) is any point of the object (i going from 1 to N)
   N is the number of points of the object
7. Storage of the centers of gravity of the 3 largest detected objects.
8. Labelling of the 3 objects (A, B and C).
9. Rotation among A, such as [A,B] becomes horizontal.
10. Affinity along the X axis, such as : Dist(A,B) = L.
11. Skew along the Y axis, such as [A,C] becomes vertical.
12. Affinity along the Y axis, such as : Dist(A,C) = l.
    We thus obtain a matrix that will describe a transformation such as :
    x' = a*x + b*y + c
    y' = d*x + e*y + f
13. Applying of the defined transformation on the image, using the backward mode, in order to be sure to affect every pixel of the destination frame.

Figure 5. On the acquired image (top), the fiducials could be located at any position on the image, but they form an orthonormal marker before the cutting procedure. A first-order affine transform based on the position of three laser fiducials have proved to be necessary and sufficient to model the deformations. Procedure of geometrical deformations correction (bottom).

be reconstructed at the end of the EM observation and image capture. The visualization of the four depends on the number of registered images and requires typically 1 min.

3.3.2 Measurements. We know the thickness of each cut (Bron et al. 1990) and the distance between two laser shots. We thus know the voxel size, in either the X, Y, or Z directions. It is then easy to measure the distance between any couple of points, which is visualized on the screen via a couple of user-defined cursors. The visualized block is divided into six polygons as shown in Figure 9. The system recognizes in which polygon(s) the two cursors are located, and then reconstructs their original locations in X, Y, and Z.

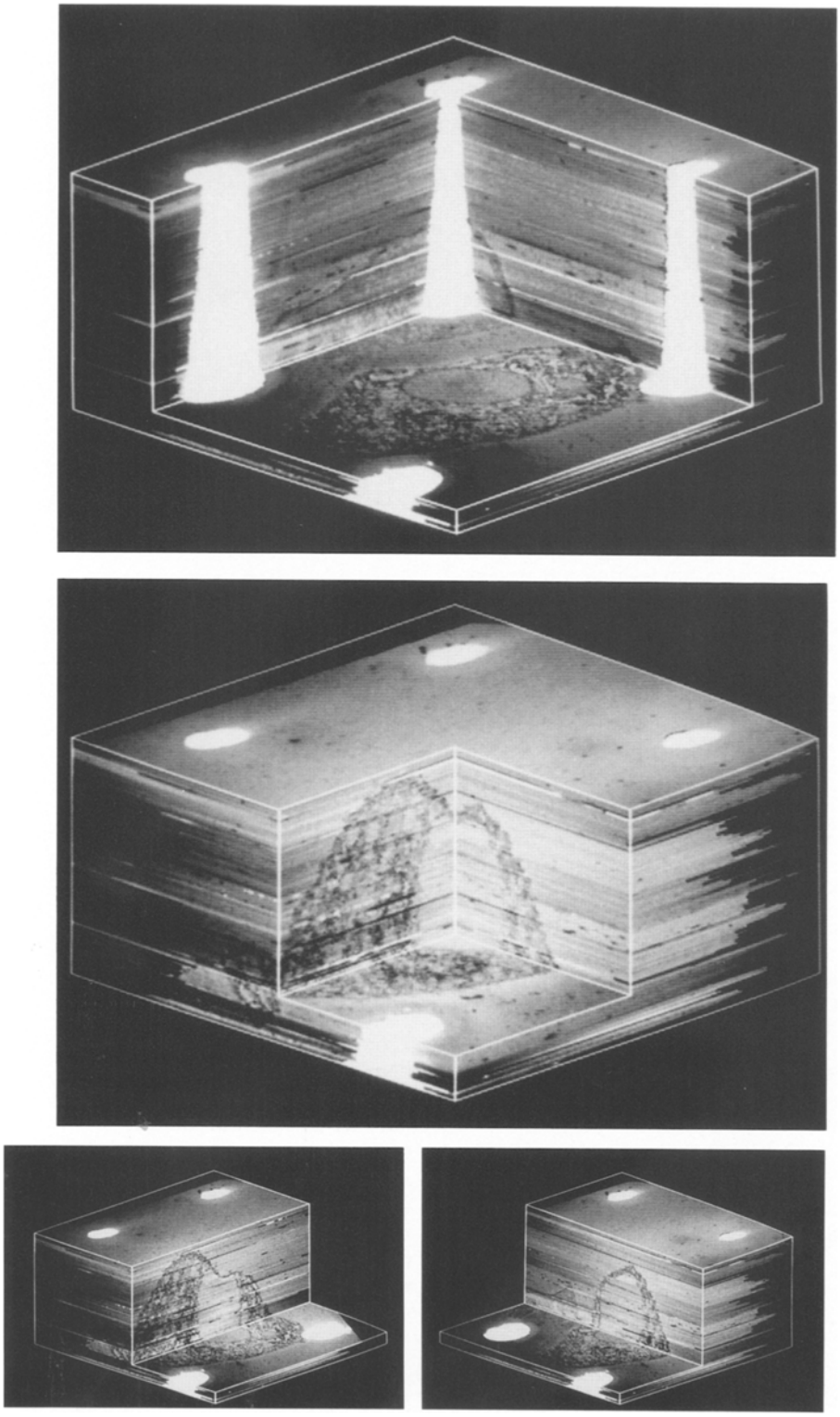

Figure 6. Examples of the reconstructed images showing the block laid open by four orthogonal sections. **(A)** The clearly visible laser holes show the precision of the registration. **(B)** The registration is applied to the cultured cell. **(C)** The presence of four frame buffers on the electronic board to produce images was intentionally used. The number of the line, the column, and the number of the cut defined four views, so that the system simultaneously built four views of the same block. Stored on the four frame buffers here is an example of two other views made during the same reconstruction step as in (B).

3.3.3 Image processing resolution. The resolution of the reconstruction is understood to be a resolution in each direction of the reconstruction:

Z resolution: The depth resolution or Z resolution depends on the thickness of the sections. With adequate cutting techniques, a depth resolution of 40 nm has been achieved. Studies under way suggest that a depth resolution of 20 nm should be routinely possible.

X resolution: The X resolution is linked to the density of digitization and to the electronic

1. Computation of the histogram of the image
2. Centering of the histogram in the grey level range. It consists of LIP-multiplcation of the values of the histogram by a given scalar, so that the mean value of the resulting histogram is 127, when values go from 0 (black) to 255 (white).
   (It forces all histograms in all images to have the same mean value.)
3. A LIP-multiplication by 2 is applied.
   (It compresses the dynamic in the light grey-levels, and expand it in the dark grey-levels (property of the LIP-multiplication).
4. Then a linear stretching of the histogram is performed, in order to fill the 0 to 255 grey-level range.
   (it expands the resulting histograms so they have roughly the same variance.)

Figure 7. Procedure of grey-level normalization.

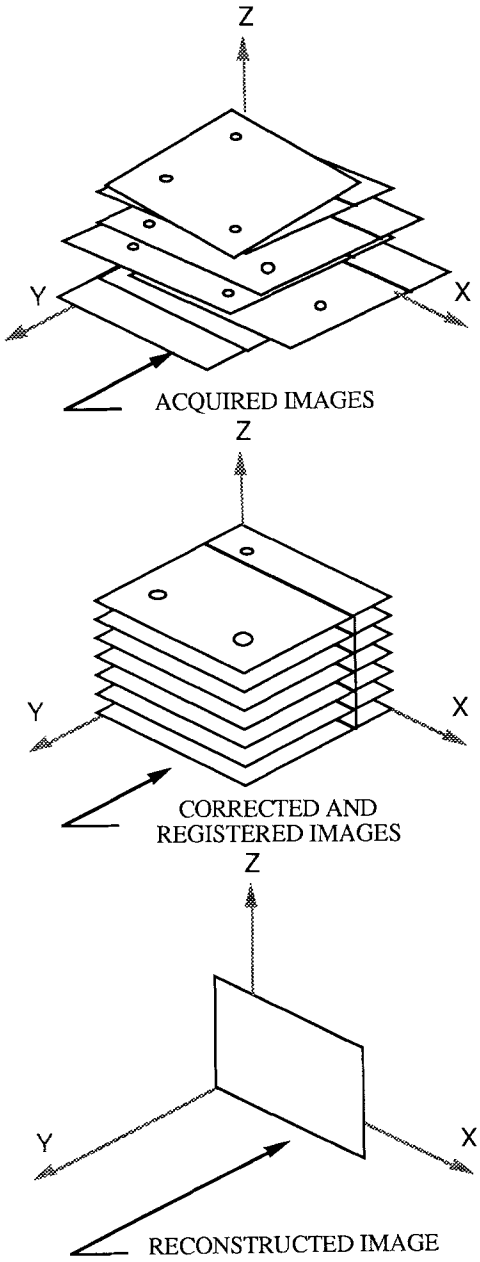

Figure 8. The extraction of a chosen line on every cut reconstructs an image having the same resolution as the original cuts and represents a new cut along another axis, exactly as if the block was cut along this direction.

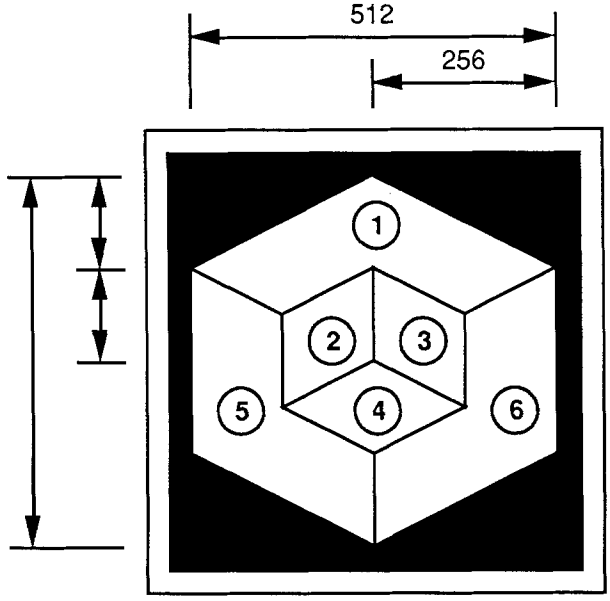

Figure 9. Cursor and measurements. The visualized block was divided into six polygons. The system recognizes in which polygon(s) the two cursors are located, and then reconstructs their original locations in *X*, *Y*, and *Z*.

spot size used in STEM. The final *X* resolution is 40 nm here, that is, the pixel length. The spot size is 40 nm and the digitization density is 512.

Y resolution: The *Y* resolution is linked to the diameter of the spot size and the number of scanning lines, in our case 40 nm and 560 lines, respectively. The signal of these lines has been digitized in 512 lines. We consider the *Y* resolution close to 40 nm.

3.3.4 Visualization resolution. The visualization screen is a 512*512-pixel map. As presented on Figure 9, the maximal possible surface used by area 1 is 65,536 pixels, which is the square of 256. This means that if we want to store the content of a 512*512-pixel digitized image in this area, we must

extract only a quarter of its information to fit in area 1. Thus, it is not possible to visualize the entire content of a 512*512 digitized image in this area. On the other hand, the optimal size of a digitized image to be fully mapped into this area is a 256*256 digitized image. Since we chose such a visualization mode, it is not necessary to store images with a resolution greater than 256*256 pixels.

Even if all the treatments performed on a digitized image are made using a 512*512-pixel resolution, the resulting images used for general observation can be stored on a hard disk using a 256*256 format. Another advantage is that a set of 128 consecutive cuts (the usual number of cuts) in a 512*512 format would need 32 Mbytes on a hard disk. Due to MS-DOS limitations, it is much more convenient to store a set of images using the 256*256 format. In our example the set of 128 cuts will need only 8 Mbytes on a hard disk.

It is possible, however, if needed to select a window of 256*256 from the original image to reach the spatial resolution of 40 nm from the original images.

4 Discussion

By using Excimer laser fiducials applied to the tissue block before sectioning, we demonstrated that electron microscopic serial sections can be automatically back-calculated for distortion, shrinkage, and orientation. Corrected images can be generated from images directly digitized from a STEM and used for three-dimensional reconstruction of entire cells of any complexity. Currently, a depth resolution of 40 nm has been achieved; studies under way suggest that a depth resolution of 20 nm should be routinely possible. These procedures already provide a new approach for obtaining precise morphometric data. Together these methods for which we use the designation CAVUM should permit a much better ultrastructural analysis of cells and cellular functions.

Present computer hardware and system have lead to compromises between visualization resolution and computation time as well as to compromises between original information and visualization features. New three-dimensional image treatment algorithms based on this concept are now under development and will be of use in the automatic extraction of cellular components. Additional features, such as rotation of the reconstructed block, sophisticated solid model shadowing, and automatic extraction of organelles requiring lengthy computations, have been done but are not routinely used. The foreseeable dramatic increase of the computation speed of low-cost computers will allow a near-real-time display of reconstructed image in any desired orientation as well as the extraction and visualization of the structures of the cell. The idea is to inspect these structures by placing a simulated observer at any location within or outside the cell.

In combination with microcomputer-controlled electron microscopes that are now also under development such a system may lead to fully automated electron microscopes. Reconstruction three-dimensional EM may then become a routine tool for biological analysis.

Acknowledgments. We are greatly indebted to Dr M. Wehner from the Fraunhofer Institute for Laser Technology (Aachen, Germany) and Dr E. Neske from Fraunhofer Institute for Measurement Techniques (Freiburg, Germany) for the laser technical assistance. We also acknowledge the expert counseling of Dr. D. Launay and the excellent technical and photographic work of Ms. Susanne Loeliger. Ms. C. Tougard (College de France) provided the cells shown in this work.

This work was supported by grants from the Swiss Federal Office of Health and Swiss National Fonds nr 31-27784.89.

References

Bron Cph, Gremillet Ph, Launay D, Jourlin M, Gautschi HP, Bächi Th, Schüpbach J (1990a) Three-Dimensional electron microscopy of entire cells. Journal of Microscopy 157(Pt 1):115–126

Bron Cph, Gremillet Ph, Launay D, Jourlin M, Gautschi HP, Bächi Th, Schüpbach J (1990b) 3D modeling of entire cells by electronic imaging. Proceedings of SPIE Meeting on Electronic Imaging, Santa Clara, CA

Jourlin M, Pinoli JC (1988) A model for logarithmic image processing. Journal of Microscopy 149(Pt 1):21–35